Physica B 449 (2014) 133–137

Contents lists available at ScienceDirect

Physica B

journal homepage: www.elsevier.com/locate/physb

Investigation of the elastic, hardness, and thermodynamic properties of actinide oxides

Wen Huang [a,*], Haichuan Chen [b]

[a] College of Electronic Engineering, Chongqing University of Post and Telecommunications, Chongqing 400065, PR China
[b] College of Electrical Engineering and Information Technology, Xihua University, Chengdu 610039, PR China

ARTICLE INFO

Article history:
Received 27 April 2014
Accepted 15 May 2014
Available online 22 May 2014

Keywords:
Elastic properties
Vickers hardness
Thermodynamic properties
Thermal conductivity

ABSTRACT

The elastic and thermodynamic properties of actinide oxides (AO_2) compounds have been investigated by using the first-principle density functional theory (DFT) within the generalized gradient approximation (GGA). The calculated lattice constants of AO_2 are in agreement with the available experiments data. The calculated elastic constants reveal that all AO_2 compounds are mechanically stable. The shear modulus, Young's modulus, Poisson's ratio σ, the ratio B/G and the anisotropy factor are also calculated. Finally, the Vickers hardness, Debye temperature, melting point and thermal conductivity have been predicted.

1. Introduction

Actinide and their oxides show many intricate physical behaviors due to the complex electronic structure properties of 5f states, and have attracted considerable attention [1,2]. Another reason for a thorough study of actinide oxides (AO_2) is their important role played in all stages of the nuclear fuel cycle. Fission yield of a uranium based conventional fission nuclear reactors can generate more than 20 fission products such as Np, Pu, Am, and Cm in the actinides [3]. The actinides affect the thermo-physical and mechanical properties, thermal conductivity, ionic diffusion and phase stability of the fuel. Therefore, thorough understandings of the physical properties of AO_2 are of great significance.

Over the past few decades, extensive studies of AO_2 have been carried out. Lu et al. [4] systematically studied the electronic, mechanical, tensile and thermodynamic properties of AmO_2 by performing density functional theory (DFT)+U calculations. Behera et al. [5] investigated the structural and mechanical properties of UO_2 using atomic level simulations. Boettger [6] predicted transition pressure of ThO_2 around 27.5 GPa by using the relativistic linear combinations of the Gaussian type orbital-fitting function technique. Wang et al. [7] studied the thermodynamic properties and the phase transition of ThO_2 from the cubic structure to the orthorhombic structure using the projector-augmented wave method. Wang et al. [8] studied the mechanical properties, electronic structure and phonon dispersion of ground state ThO_2 as well as the structure behavior up to 240 GPa. Chu et al. [9] investigated the thermal expansion coefficient, entropy, heat capacity and enthalpy of PuO_2 and α-Pu_2O_3 between 298 K and 1500 K using BMH empirical potential and shell potential. Shi et al. [10] investigated the electronic structure and optical properties of UO_2 and PuO_2 based on the DFT using the generalized gradient approximation (GGA)+U scheme. However, systematical studies on the elastic properties, Debye temperature, Vickers hardness, melting point and thermal conductivity of AO_2 are still lacking. In this paper, we present a detailed study of these physical properties of AO_2 by using the first-principle plane-wave pseudopotential (PWPP) method.

2. Calculation methods

The first-principle calculations were carried out by using the PWPP method within DFT [11]. For the exchange and correlation terms, the revised Perdew–Burke–Ernzerhof (rPBE) [12] was used within the GGA. Using the PWPP method, $2s^22p^4$ for O, $6d^17s^2$ for Ac, $6s^26p^66d^27s2$ for Th, $5f^26s^26p^66d^17s^2$ for Pa, $5f^36s^26p^66d^17s^2$ for U, $5f^46s^26p^66d^17s^2$ for Np, $5f^66s^26p^67s^2$ for Pu, $5f^76s^26p^67s^2$ for Am, $5f^76s^26p^66d^17s^2$ for Cm, $5f^96s^26p^67s^2$ for Bk, $5f^{10}6s^26p^67s^2$ for Cf, $5f^{11}6s^26p^67s^2$ for Es, $5f^{12}6s^26p^67s^2$ for Fm, $5f^{13}6s^26p^67s^2$ for Md and $5f^{14}6s^26p^67s^2$ for No were treated explicitly as valence electrons. Plane wave cut-off energy of 800 eV and an $8\times8\times8$ grid of Monkhorst–Pack points have been employed in this study to ensure well convergence of the computed structures and energies. The structural parameters of AO_2 were calculated

* Corresponding author. Tel.: +86 13638332471; fax: +86 23 63962314.
E-mail address: huangwen@cqupt.edu.cn (W. Huang).

http://dx.doi.org/10.1016/j.physb.2014.05.024
0921-4526/

by using the Broyden–Fletcher–Goldfarb–Shanno (BFGS) [13–16] method.

3. Results and discussions

3.1. Structural properties

At ground state, all AO_2 crystallize in face-centered cubic CaF2-like (space group Fm-3m) structure. Their cubic unit cells are composed of four AO_2 formula units with the actinide atom and the O atom in 4*a* and 8*c* sites, respectively. In this arrangement, each actinide atom is located at the face-centered positions, together with eight O atoms which fill tetrahedral sites (Fig. 1). The lattice constants of AO_2 are summarized in Table 1. The calculated lattice constants of AO_2 are in good agreement with the available experiments data. The deviations from the experimental data are underestimated by less than 3.3%. These results show and confirm that the method used in this study is reliable, thereby the optimized lattice constants can be used for future calculations of other parameters.

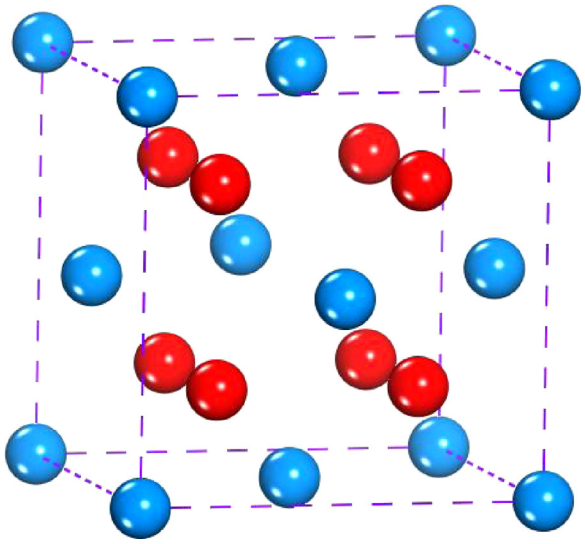

Fig. 1. The cubic structures of AO_2; A atoms are shown in blue, and O atoms in red. (For interpretation of the references to color in this figure legend, the reader is referred to the web version of this article.)

Table 1
Calculated lattice constants together with experimental data.

Compounds	Pearson symbol	*a* (Å)		*ρ* (g/cm^3)	
		Cal.	Exp.	Cal.	Exp.
AcO_2	*cF*12	5.20752		12.1818	
ThO_2	*cF*12	5.62802	5.695[a]	9.83795	9.49492
PaO_2	*cF*12	5.41799	5.505[b]	10.9837	10.4482
UO_2	*cF*12	5.4204	5.444[c]	11.2622	11.1164
NpO_2	*cF*12	5.36279	5.434[d]	11.5847	11.1475
PuO_2	*cF*12	5.34571	5.3955[e]	12.0005	11.6713
AmO_2	*cF*12	5.32492	5.376[f]	12.0976	11.7652
CmO_2	*cF*12	5.31354	5.357[g]	12.3526	12.0544
BkO_2	*cF*12	5.30981	5.332[h]	12.3787	12.2385
CfO_2	*cF*12	5.32380	5.31[i]	12.4574	12.5548
EsO_2	*cF*12	5.35226		12.3031	
FmO_2	*cF*12	5.39806		12.2037	
MdO_2	*cF*12	5.46707		11.7880	
NoO_2	*cF*12	5.54886		11.3132	

[a] Ref. [17].
[b] Ref. [18].
[c] Ref. [19].
[d] Ref. [20].
[e] Ref. [21].
[f] Ref. [22].
[g] Ref. [23].
[h] Ref. [24].
[i] Ref. [25].

3.2. Single-crystal elastic constants

Elastic constants of crystals provide a link between mechanical and dynamical behaviors. Also, they give important information concerning the elastic response of a crystal to an external pressure. To calculate the elastic constants, we have applied the non-volume-conserving method.

The mechanical stability of AO_2 is studied by the calculated elastic constants. For the cubic crystals, the mechanical stability criteria are given by [26]

$$\left\{\begin{array}{l} C_{11}>0; C_{44}>0 \\ C_{11}-C_{12}>0 \\ C_{11}+2C_{12}>0 \end{array}\right\} \quad (1)$$

The calculated elastic constants of AO_2 at 0 GPa are shown in Table 2. For comparison, the available experimental data and theoretical results by others are also presented. According to Eq. (1), it should be noted that AO_2 are mechanically stable. In Table 2, it can be noted that the calculated values of C_{11} and C_{12} for UO_2 are slightly lower than the corresponding experimental ones [27] with deviations of 6.6% and 28.9%, respectively. For ThO_2, the calculated values are in good agreement with the experimental results with the maximum deviation of 13.7% [28]. We also found the calculative value of C_{44} is larger than the experimental value, presumably because oxygen relaxation was not included.

3.3. Polycrystalline elastic moduli

In the particular case of randomly oriented polycrystals, one may evaluate aggregate average elastic properties based on additional hypotheses such as isostress named as Reuss or Voigt states. For the cubic structure, the shear modulus *G* and the bulk modulus *B* are given for each approximation by [26]

$$\left\{\begin{array}{l} G_V=\frac{1}{5}(C_{11}-C_{12}+3C_{44}) \\ B_V=B_R=\frac{1}{3}(C_{11}+2C_{12}) \\ G_R=\frac{5C_{44}(C_{11}-C_{12})}{4C_{44}+3(C_{11}-C_{12})} \end{array}\right\} \quad (2)$$

To make further conclusions on the mechanical properties, polycrystalline bulk modulus B_H, shear modulus G_H, Young's modulus *E* and Poisson's ratio σ have been calculated by the Voigt–Reuss–Hill approximation [37,38]:

$$\left\{\begin{array}{l} G_H=\frac{1}{2}(G_V+G_R) \\ B_H=\frac{1}{2}(B_V+B_R) \\ E=\frac{9B_HG_H}{3B_H+G_H} \\ \sigma=\frac{3B_H-2G_H}{2(3B_H+G_H)} \end{array}\right\} \quad (3)$$

Using Eqs. (2) and (3) the calculated bulk modulus *B*, shear modulus *G* and Young's modulus *E* for AO_2 are presented in Table 3. The experimental data and calculated results are included for comparison. The polycrystalline elastic modulus obtained in our work is found to in good agreement with the previous results. The deviations are partly due to temperature, volume effects and different DFT approximation (LDA or GGA). Bulk modulus measures the resistance that material offers to change in its volume. From Table 3, we can see that the bulk modulus of AcO_2 is larger than the others, indicating that AcO_2 is less compressible than the